MoS_2-HgTe Quantum Dot Hybrid Photodetectors beyond 2 µm

*Nengjie Huo[1], Shuchi Gupta[1], Gerasimos Konstantatos[1,2]**

[1]ICFO – Institut de Ciencies Fotoniques, The Barcelona Institute of Science and Technology, Castelldefels, 08860, Barcelona, Spain

[2]ICREA – Institució Catalana de Recerca i Estudis Avançats, Lluis Companys 23, 08010 Barcelona, Spain

E-mail: (Gerasimos.konstantatos@icfo.es)

Keywords: MoS_2, HgTe quantum dot, infrared photodetector, phototransistors, photoconductive gain

Abstract: Mercury telluride (HgTe) colloidal quantum dots (CQDs) have been developed as promising materials for the short and mid-wave infrared photodetection applications because of their low cost, solution processing and size tunable absorption in the short wave- and mid-infrared spectrum. However, the low mobility and poor photo-gain have limited the responsivity of HgTe CQDs-based photodetectors to only tens of mA/W. Here, we integrated HgTe CQDs on a TiO_2 encapsulated MoS_2 transistor channel to form hybrid phototransistors with high responsivity of ~10^6 A/W, the highest reported to date for HgTe QDs. By operating the phototransistor in the depletion regime enabled by the gate modulated current of MoS_2, the noise current is significantly suppressed leading to an experimentally measured specific detectivity D* of ~10^{12} Jones at a wavelength of 2 µm. This work demonstrates for the first time the potential of the hybrid 2D/QD detector technology in reaching out to wavelengths beyond 2 µm with compelling sensitivity.

Infrared (IR) photodetectors in the short-wave infrared (SWIR, 1-2 μm), mid-wave infrared (MWIR, 2-5 μm), and long wave infrared (LWIR, 8-12 μm)) are of increasing technological importance for applications in night vision, remote sensing and environmental monitoring.[1-3] Although commercial IR photodetectors exist, these are based on epitaxially grown material systems such as InGaAs, InAs, HgCdTe, and type-II super-lattices; HgCdTe, also called MCT (Mercury-Cadmium-Telluride), can be tuned to any cut-off wavelength from the LWIR to the SWIR by tuning the stoichiometric composition.[4, 5] As a result of the involved growth mechanisms the cost of these technologies along with their CMOS incompatibility pose significant challenges in the exploitation of IR sensing for this increasing number of applications. To address these challenges, colloidal quantum dots (CQDs) with small bandgap[6-10] have been extensively studied as an alternative low-cost, CMOS-compatible optoelectronic platform for IR detectors.[11] HgSe and HgTe colloidal quantum dots, in particular, have been considered for IR detection due to their small, tunable bandgap through the full infrared spectrum[12-16] with very favourable optical properties.[13-21] Photoconductive detectors based on those QDs have also been reported based on spin-coating, spray-casting or inkjet-printing techniques on integrated electrode structures.[12, 22-28] The responsivity in those prior reports, however, has been limited to tens of mA/W due to the low carrier mobility, lack of sensitizing centers and the consequent absence of photoconductive gain in contrast to what has been extensively reported in PbS-based CQD photoconductors.[6, 11] Recently, with the advent of 2D materials, the combination of graphene or semiconducting transition metal dichalcogenides (TMDs) with quantum dots in phototransistor architectures have led to new records of gain and sensitivity. These detectors exploit the synergy of strong, tunable absorption and sensitization of QDs with the atomically thin, high mobility channels of 2D materials to offer photoconductive gains on the order of 10^5 - 10^8 employing PbS CQDs for a wavelength range up to 1650 nm.[29-31] The use of semiconducting 2D channels is of particular promise for they enable the operation of the transistor in the depletion mode, offering thus the advantage of low

leakage current in dark conditions with appropriate interface engineering.[32] This feature is of paramount importance especially in low-bandgap IR photodetectors that suffer from large dark currents and therefore large noise currents at room temperature.

Prerequisite features of high performance infrared detectors include strong and fast photo-response, low noise as well as broadband spectrum coverage. To accommodate these features in a single platform with the added value of low-cost, CMOS integrability and potential flexibility, we designed novel MoS_2/HgTe QDs hybrid architectures. A critical layer for addressing those challenges in those structures is a TiO_2 buffer layer between the MoS_2 channel and the HgTe QD layer that serves as a protective layer of the MoS_2 channel and as an n-type electron acceptor medium to form an efficient p-n junction with the HgTe QDs at the interface facilitating the charge transfer to MoS_2 channel. Thus, a gate modulated low dark current can be achieved. At the same time, high responsivity is reported thanks to a carrier recirculation mechanism which leads to the first demonstration of gain in HgTe QD – based materials. More interestingly, the response spectrum of our hybrid photodetectors is extended to short infrared wavelength range beyond 2 μm with the potential for further extension depending on the size of HgTe QDs. Considering the long wavelength light absorption up to 20 μm reported for mercury chalcogenides QDs,[15, 21] this hybrid platform paves the way to high performance, high-gain, and low-cost mid- and long-wave infrared photodetectors.

Figure 1a shows the optical microscope (OM) and SEM images of the MoS_2/TiO_2/HgTe hybrids photodetectors. The schematic diagram of the device architecture is shown in Figure 1b. We started the fabrication of the devices by exfoliating few layer of MoS_2 on the SiO_2/Si (285 nm) substrate, the source-drain electrodes of Ti/Au were then fabricated using the photolithography and electron beam deposition technique. Then one thin TiO_2 buffer layer was deposited by atomic layer deposition. Finally we spin-coated HgTe CQDs on top of the devices employing a layer by layer process to yield a thickness of 80-90 nm. This thickness has been chosen for it yielded optimized performance with PbS QD solids, yet this is not necessarily the

optimum thickness for HgTe QDs; thus the reported devices are not considered optimized.[33] The detailed description of the materials synthesis and device fabrication can be seen in the Experimental part. The OM images of the devices after each step are shown in Figure S1 and the electrical and photodetection properties were measured in ambient environment and room temperature.

We firstly focus on the electronic transfer characteristics of the hybrid phototransistors as shown in the Figure 1c. The pristine MoS_2 exhibits excellent gate modulated current with high on/off ratio of 10^7 and large calculated mobility of 18 cm^2/Vs. After the ALD deposition of TiO_2, the MoS_2 field effect transistors (FETs) performance was maintained but with decreased threshold voltage, suggesting an n-type doping effect for the MoS_2 due to the removal of adsorbates or oxygen vacancies in nonstoichiometric TiO_2 film.[32] TiO_2 is widely studied n-type semiconductor with large band gap of 3.2 eV and low mobility which can act as transparent window for vis/IR light and has negligible current leakage through this layer.[34] Upon deposition of HgTe QDs on the TiO_2 encapsulated MoS_2 channel, the hybrids device preserves well gate modulated current with low off-current (~pA) and high on-current (~10 μA) closed to that in the pristine MoS_2. The increased threshold voltage indicates the p-type doping effect. The HgTe QDs demonstrate p-type behaviour with low mobility as evidenced from the transfer characteristics of HgTe only transistors (Figure S2). Thus a built-in potential would be formed as a result of the p-n junction between HgTe and MoS_2/TiO_2, which in turn facilitates the photo-generated charge transfer from the QDs to the MoS_2 channel. To showcase the critical role of the TiO_2 layer we fabricated devices in the absence of it. The MoS_2/HgTe devices lose the large current modulation depth yielding very low on/off ratio of about 10 (Figure 1c). The resultant phototransistors cannot be turned off in the depletion region even by adding large negative back gate compromising the high sensitivity. The loss of the gate modulation is attributed to the formation of large density of states within the band gap of the MoS_2 from the direct cross-

linking with the QDs at the interface.[30] However, the presence of the TiO_2 buffer layer suppresses this interaction and preserves the FETs performance characteristic of MoS_2.[32]

From ultraviolet photoelectron spectroscopy (UPS) measurement (Figure S3), the energy band of HgTe QDs has been determined, which forms a type-II band alignment with TiO_2/MoS_2 as shown in **Figure 2**a. Upon light illumination on the HgTe QDs, the photo-generated electrons are transferred into the MoS_2 channel through the thin TiO_2 layer due to the built-in field while the holes remain trapped in the QDs layer with a timescale of τ_{life}. By applying the source-drain bias, the transferred electrons are drifted to the drain within a timescale of $\tau_{transit}$. Considering the high mobility of MoS_2 (~18 cm^2/Vs) and the channel length (~5 μm), the carrier transit time is orders of magnitude shorter than the trapping lifetime in the quantum dots. Thus multiple electrons are recirculated in the MoS_2 channel following a single electron-hole photo-generation, leading to a photoconductive gain defined as $G = \frac{\tau_{life}}{\tau_{transit}}$. Here $\tau_{transit} = \frac{L^2}{\mu V_{sd}} = 9\ ns$, where L is length of the channel, μ is the mobility and V_{sd} is the applied bias. τ_{life} can be extracted from the temporal response of the hybrids photodetectors, which is around 4 ms for 1310 nm wavelength light (Figure 2c) leading to a photoconductive gain on the order of 10^6. The carrier lifetime is most likely determined by trap-assisted (indirect) recombination through the traps or defect levels in TiO_2 or HgTe layer and can be further optimized upon further trap-state passivation.

The resultant responsivity, defined as $R = {I_{ph}}/{PS}$, where I_{ph} is the photocurrent, P is the incident light power density and S is the active area, is shown in Figure 2b as a function of the incident optical power. To clearly demonstrate the improvement of the performance of the hybrid photodetectors, we made control devices based on HgTe QDs only and neat MoS_2 devices with same active area and characterized under the same measurement conditions. The responsivity of the hybrid devices can reach up to 10^6 A/W under weak optical power density of 0.35 μW/cm^2 (70 fW on active area), which is improved by seven orders of magnitude

compared to HgTe QD only devices. Figure 2b shows the light power dependence of responsivity of different devices with V_{sd} of 1 V and 0 backgate voltage. The poor responsivity of HgTe QD detectors results from the low mobility of QD films (2×10^{-3} cm^2/Vs). In all cases, the responsivity decreases with increasing illumination intensity which can be due to the progressive saturation of photo-sensitizing traps, intrinsic Auger recombination in HgTe QDs layers in view of the very long carrier lifetimes or the produced inverse electrical field which can accelerate the carrier recombination at the interface.[29, 30]

The time traces of photocurrent of different devices are illustrated in Figure 2c. For pristine MoS_2, the defects or adsorbates such as oxygen and H_2O can be responsible for the very slow photo-response (Figure S4) as previously documented for MoS_2 detectors.[35] After the ALD deposition of TiO_2, the response is improved to around 2 s (Figure 2c) similar to the ALD HfO_2 encapsulated MoS_2.[36] However, the spectral coverage of TiO_2 encapsulated MoS_2 devices is limited to the visible-near infrared range determined by the band gap of the multilayer MoS_2 (Figure 2d). HgTe CQD detectors demonstrate fast photoresponse with decay time of less than 4 ms, limited by the measurement system resolution, but with very low responsivity in accordance with prior reports[22-28] (Figure 2d). On the other hand, the hybrid phototransistors demonstrate the combined features of speedy response of HgTe QD photodetectors with high gain across the VIS-SWIR (Figure 2d) following the absorption spectrum of HgTe QDs.

The presence of backgate in these detectors can act as a sensitivity knob to boost the detectivity by operating the detector in the depletion regime, i.e. the regime in which the dark current in the channel is minimized. To identify the maximum sensitivity point we plot in **Figure 3**a the responsivity, the light-to-dark current ratio and the experimental D* defined as $D^* = \frac{\sqrt{AB}}{NEP} = \frac{R\sqrt{A}}{S_n}$, where *NEP* is the noise equivalent power, *R* is the responsivity, *A* is the active area of the detector, *B* is the noise bandwidth and S_n is the noise spectral density of the detector, as function of the backgate voltage. The noise spectral densities measured at different backgate

voltages, used to calculate the D* at these points are shown in Figure 3b. A 1/f-noise component is observed, akin to 2D materials due to the non-ohmic contacts and edge defects.[37, 38] At the optimum backgate, the noise spectral density S_n, extracted at the measured bandwidth of 1 Hz, is 3.5×10^{-13} A/$\sqrt{Hz}$, on par with the noise current of the HgTe QD-only devices. Thus the sensitivity of the hybrid detectors over that of the QD-only detectors scales with the responsivity ratio and is approximately 4 orders of magnitude higher (Figure S5). While the responsivity decreases with operating the detector in the depletion regime, the sensitivity of the detector improves dramatically in view of the orders-of-magnitude reduction of the noise current. The responsivity spectra at different backgate voltages are plotted in Figure 3c. For a typical hybrid device, the responsivity at V_{sd} of 1 V and V_g of -15 V with light power density of 0.35 μW/cm^2 is 5×10^3 A/W, the measured bandwidth is 1 Hz and the active area is 20 μm^2, thus the specific D* is calculated to be 6.4×10^{12} Jones in the visible, at a frequency of 1 Hz. In view of the detectors´ fast response and the reduction in noise at higher frequencies the D* further increases by almost 50% up to a modulation frequency of 20 Hz (Figure S6). Figure 3d shows the spectral detectivity of hybrid detectors at V_{sd} of 1 V and V_g of -15 V showing the high detectivity of around 10^{12} Jones in the short-wave infrared of 2 μm. The D* in the whole spectrum is four orders of magnitude higher compared to that of HgTe only detectors (Figure S5). For the latter, an increase in applied bias can increase the responsivity up to 2 A/W; the noise current density though also increased to 1.5×10^{-11} A/$\sqrt{Hz}$ yielding a detectivity of 10^7-10^8 Jones (Figure S7).

In summary, we have demonstrated hybrid 2D-QD photodetectors based on MoS_2 and HgTe QDs with experimentally measured D* of 10^{12} Jones at 2 μm and at room temperature, two orders of magnitude higher than prior reports from HgTe-based photodetectors (Table S1 in SI) as well as existing commercially available technologies based in extended-InGaAs, InAs or HgCdTe that also require thermo-electric cooling (see Table S2 in SI). We have also demonstrated for the first time gain on the order of 10^6 and responsivity up to 10^6 A/W in HgTe QD based photodetectors. That was achieved through hybridization with a 2D MoS_2 transistor

channel in which HgTe QDs acted as a sensitizing layer. The reported D* is currently limited by 1/f noise in the MoS_2 channel. Future efforts to identify and suppress 1/f noise in 2D materials may lead to even higher sensitivities. These findings pave the way for the implementation of high sensitivity, low cost SWIR and mid-IR detectors with compelling performance operating at room temperature.

Experimental Section

HgTe CQDs synthesis:

0.128 g of Te pallets were added to 1 ml of trioctylphosphine (TOP). The solution was subsequently heated at 100 ^{0}C to form a clear yellowish solution. This Te-TOP solution was stored in glove box for further use. 100 µl of this solution was diluted with 5 ml of oleylamine for synthesis of HgTe nanoparticles. Note that oleylamine for this purpose was previously dried at 80 ^{0}C under vacuum overnight. In a separate flask, 54 mg of $HgCl_2$ was mixed with 8 ml of oleylamine. The solution was heated to 80 ^{0}C under vacuum for an hour and later switched to Argon. Further, $HgCl_2$-Oleylamine solution was heated to 90 ^{0}C and a solution of Te-TOP-oleylamine was added immediately. The reaction time was adjusted according to the desired final size of nanoparticles. After the synthesis, the nanocrystals were stabilized with 100 µl of TOP and 1 ml dodecanethiol. The nanocrystals were washed twice with a mixture of methanol and acetone.

Device fabrication and measurement:

The MoS_2 crystals were purchased from the 2D semiconductors corporation. The few layer MoS_2 was then exfoliated with PDMS tape on Si/SiO_2 (285 nm) wafer using the micromechanical exfoliation method. The detailed process is as follows: The MoS_2 crystal slices were pasted on PDMS adhesive tape. Folding the sticky side of the tape in half then tearing the tape very slowly. Repeating this operation for 2-3 times then exfoliating the

nanoflakes onto SiO_2/Si substrate by pressing the tape gently and removing it slowly. Finally, put the substrate into acetone for 2 hours at 60 ^{0}C to remove the residual glue.

Metal contacts were fabricated by the laser writing lithography, and Ti (2 nm) and Au (70 nm) electrodes were evaporated by e-beam and thermal evaporation, respectively. After test measurements in ambient conditions the devices were covered by 20 nm TiO_2 with an atomic layer deposition technique (Savannah 200, Cambridge Nanotech). Titanium isopropoxide and H_2O precursors were used alternating with open valve times of 0.1 and 0.015 s, respectively, separated by a 10 s pump time. The growth rate and temperature were set to be 0.04 nm/cycle and 200 degrees.

The HgTe QDs film was then spin-coated in a standard layer-by-layer approach at a rotation speed of 3000 rpm. The QDs concentration used was 30 mg/mL in toluene, and the EDT solution for ligand exchange was 2 vol % in acetonitrile. Toluene and acetonitrile were used to rinse the device after each layer of QDs and EDT deposition. The resulting thickness of the samples was in the range 80-90 nm.

All the measurements were performed in ambient conditions using an Agilent B1500A semiconducting device analyzer. For spectral photo-response measurements the devices were illuminated with fiber-coupled and spectrally filtered light from a supercontinuum light source (SuperKExtreme EXW-4, NKT Photonics). Responsivity and temporal response times were measured under short-pulsed light at a wavelength of 635 nm or 1310 nm from a four-channel laser controlled with an Agilent A33220A waveform generator. Several dark current traces were measured with the Agilent system (Agilent B1500A) under exactly the same conditions as the optical measurements were performed (same V_g and V_{sd}) at a sampling rate of 50 Hz. We obtained the noise spectral density by calculating the Fourier transformation of dark current traces. As the photocurrent and responsivity were measured at a light modulation frequency of 1 Hz, thus the noise current spectral density was extracted at 1 Hz to calculate the corresponding detectivity D* (1 Hz).

Supporting Information

Supporting Information is available from the Wiley Online Library or from the author.

Acknowledgements

We acknowledge funding from Fundació Privada Cellex, and European Commission's Seventh Framework Programme under Graphene Flagship (contract no. CNECT-ICT-604391). We also acknowledge financial support from the Spanish Ministry of Economy and Competitiveness (MINECO) and the "Fondo Europeo de Desarrollo Regional" (FEDER) through grant MAT2014-56210-R. This work was also supported by AGAUR under the SGR grant (2014SGR1548). G.K. acknowledges financial support from the Spanish Ministry of Economy and Competitiveness, through the "Severo Ochoa" Programme for Centres of Excellence in R&D (SEV-2015-0522).

References

[1] J.-E. Källhammer, *Nat. Photonics* **2006**, *sample issue*, 12.

[2] S. Kim, Y. T. Lim, E. G. Soltesz, A. M. D. Grand, J. Lee, A. Nakayama, J. A. Parker, T. Mihaljevic, R. G. Laurence, D. M. Dor, L. H. Cohn, M. G. Bawendi, J. V. Frangioni, *Nat. Biotechnol.* **2004**, *22*, 93.

[3] J. M. Kahn, J. R. Barry, *Proc. IEEE* **1997**, *85*, 265.

[4] A. Rogalski, *Infrared Phys. Technol.* **2002**, *43*, 187.

[5] A. Rogalski, J. Antoszewski, L. Faraone, *J. Appl. Phys.* **2009**, *105*, 091101.

[6] G. Konstantatos, I. Howard, A. Fischer, S. Hoogland, J. Clifford, E. Klem, L. Levina, E. H. Sargent, *Nature* **2006**, *442*, 180.

[7] D. Talapin, C. B. Murray, *Science* **2005**, *310*, 86.

[8] G. Konstantatos, C. Huang, L. Levina, Z. Lu, E. H. Sargent, *Adv. Funct. Mater*. **2005**, *15*, 1865.

[9] S. A. McDonald, G. Konstantatos, S. Zhang, P. W. Cyr, E. J. D. Klem, L. Levina, E. H. Sargent, *Nature Mater.* **2005**, *4*, 138.

[10] M. Bernechea, N. Cates Miller, G. Xercavins, D. So, A. Stavrinadis, G. Konstantatos, *Nat. Photonics* **2016**, *10*, 521.

[11] G. Konstantatos, J. P. Clifford, L. Levina, E. H. Sargent, *Nat. Photonics* **2007**, *1*, 531.

[12] E. Lhuillier, S. Keuleyan, P. Rekemeyer, P. Guyot-Sionnest, *J. Appl. Phys.* **2011**, *110*, 033110.

[13] E. Lhuillier, S. Keuleyan, H. Liu, P. Guyot-Sionnest. *Journal of Elec. Mater*. **2012**, *41*, 2725.

[14] E. Lhuillier, S. Keuleyan, P. Guyot-Sionnest, *Chem. Mater.* **2013**, *25*, 1272.

[15] S. E. Keuleyan, P. Guyot-Sionnest, C. Delerue, G. Allan, *ACS Nano* **2014**, *8*, 8676.

[16] E. Lhuillier, S. Keuleyan, P. Zolotavin, P. Guyot-Sionnest, *Adv. Mater.* **2013**, *25*, 137.

[17] M. K. Jana, P. Chithaiah, B. Murali, S. B. Krupanidhi, K. Biswas, C. N. R. Rao, *J. Mater. Chem. C* **2013**, *1*, 6184.

[18] A. Rogach, S. Kershaw, M. Burt, M. Harrison, A. Kornowski, A. Eychmüller, H. Welle, *Adv. Mater.* **1999**, *11*, 552

[19] M. T. Harrison, S. V. Kershaw, A. L. Rogach, A. Kornowski, A. Eychmüller, H. Welle, *Adv. Mater.* **2000**, *12*, 123.

[20] A. L. Rogach, D. S. Koktysh, M. Harrison, N. A. Kotov, *Chem. Mater.* **2000**, *12*, 1526.

[21] E. Lhuillier, M. Scarafagio, P. Hease, B. Nadal, H. Aubin, X. Z. Xu, N. Lequeux, G. Patriarche, S. Ithurria, B. Dubertret, *Nano Lett.* **2016**, *16*, 1282.

[22] M. Chen, H. Yu, S. V. Kershaw, H. Xu, S. Gupta, F. Hetsch, A. L. Rogach , N. Zhao, *Adv. Funct. Mater.* **2014**, *24*, 53.

[23] S. Keuleyan, E. Lhuillier, V. Brajuskovic, P. Guyot-Sionnest, *Nat. Photonics* **2011**, *5*, 489.

[24] M. Böberl, M. V. Kovalenko, S. Gamerith, E. J. W. List, W. Heiss, *Adv. Mater.* **2007**, *19*, 3574.

[25] P. Guyot-Sionnest, J. Andris Roberts, *Appl. Phys. Lett.* **2015**, *107*, 253104.

[26] Z. Deng, K. S. Jeong, P. Guyot-Sionnest, *ACS Nano* **2014**, *8*, 11707.

[27] K. S. Jeong, P. Guyot-Sionnest, *ACS Nano* **2016**, *10*, 2121.

[28] M. K. Jana, P. Chithaiah, B. Murali, S. B. Krupanidhi, K. Biswas, C. N. R. Rao, *J. Mater. Chem. C* **2013**, *1*, 6184.

[29] G. Konstantatos, M. Badioli, L. Gaudreau, J. Osmond, M. Bernechea, F. P. Garcia de Arquer, F. Gatti, F. H. L. Koppens, *Nat. Nanotechnol.* **2012**, *7*, 363.

[30] D. Kufer, I. Nikitskiy, T. Lasanta, G. Navickaite, F. H. L. Koppens, G. Konstantatos, *Adv. Mater.* **2015**, *27*, 176.

[31] I. Nikitskiy, S. Goossens, D. Kufer, T. Lasanta, G. Navickaite, F. H. L Koppens, G. Konstantatos, *Nat. Commun.* **2016**, 7, 11954.

[32] D. Kufer, T. Lasanta, M. Bernechea, F. H. L. Koppens, G. Konstantatos, *ACS Photonics* **2016**, *3*, 1324.

[33] D. Zhitomirsky, O. Voznyy, S. Hoogland, E. H. Sargent, *ACS Nano* **2013**, *7*, 5282.

[34] D. A. R. Barkhouse, R. Debnath, I. J. Kramer, D. Zhitomirsky, A. G. Pattantyus-Abraham, L. Levina, L. Etgar, M. Grätzel, E. H. Sargent, *Adv. Mater.* **2011**, *23*, 3134.

[35] O. Lopez-Sanchez, D. Lembke, M. Kayci, A. Kis, *Nat. Nanotechnol.* **2013**, *8*, 497.

[36] D. Kufer, G. Konstantatos, *Nano Lett.* **2015**, *15*, 7307.

[37] J. Renteria, R. Samnakay, S. L. Rumyantsev, C. Jiang, P. Goli, M. S. Shur, A. A. Balandin, *Appl. Phys. Lett.* **2014**, *104*, 153104.

[38] H.-J. Kwon, H. Kang, J. Jang, S. Kim, C. P. Grigoropoulos, *Appl. Phys. Lett.* **2014**, *104*, 083110.

Figures

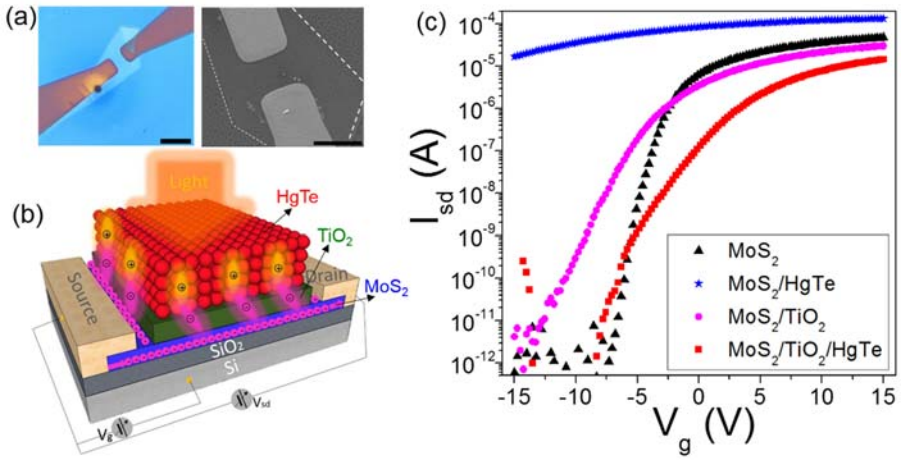

Figure 1. (a) Optical microscope and SEM images of typical $MoS_2/TiO_2/HgTe$ hybrid photodetectors, both scale bars are 5 μm. (b) Schematic diagram of the hybrids device with light illumination and of the photo-generated carrier separation and transport in the hybrids photodetectors (c) Transfer curves of pristine MoS_2 and $MoS_2/HgTe$ with and without TiO_2 photodetectors, the device without the ALD TiO_2 layer lost the gate modulation with high dark current, but the current remains low with TiO_2 layer. The applied bias is 1 V.

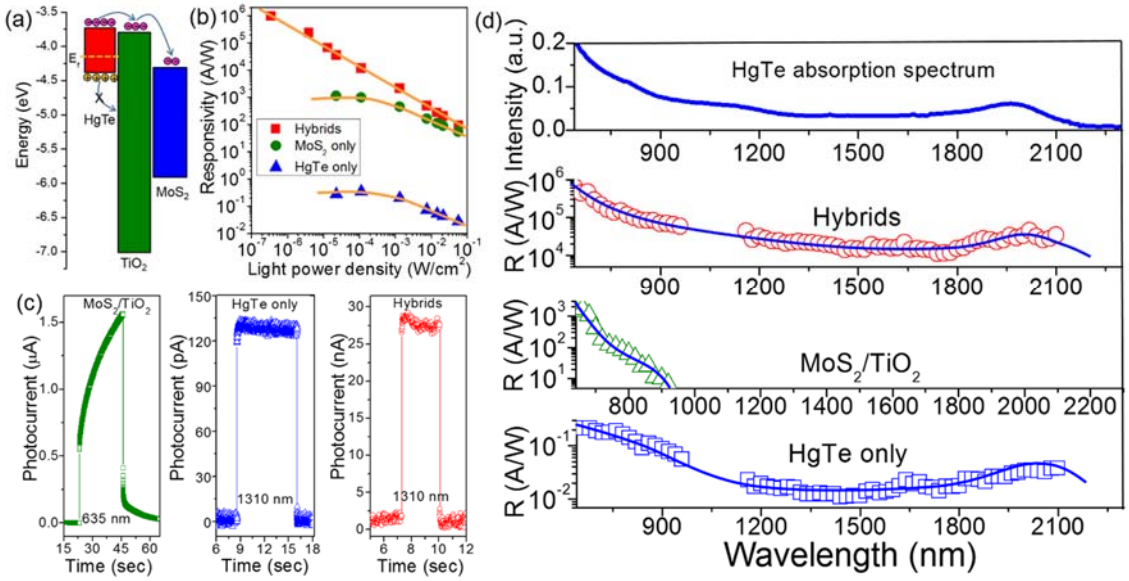

Figure 2. (a) Band alignment of MoS_2, TiO_2 and HgTe QDs, performing type-II band alignment at the HgTe/TiO_2 interface. (b) Light power density dependence of the responsivity of MoS_2, HgTe and hybrids photodetectors, the light wavelength is 635 nm, the applied bias and gate are 1 V and 0 V, respectively. (c) Dynamic response of photocurrent in different devices with light wavelength of 635 nm (56.2 mW/cm^2) and 1310 nm (53 mW/cm^2), respectively, exhibiting sub-milliseconds response. (d) Spectral responsivities for three devices, the hybrid detectors show extended detection wavelength up to 2.1 μm and enhanced responsivity following the absorption spectrum of HgTe QDs. The applied bias and gate are 1 V and 0 V, respectively. The blue line is a guide to the eye.

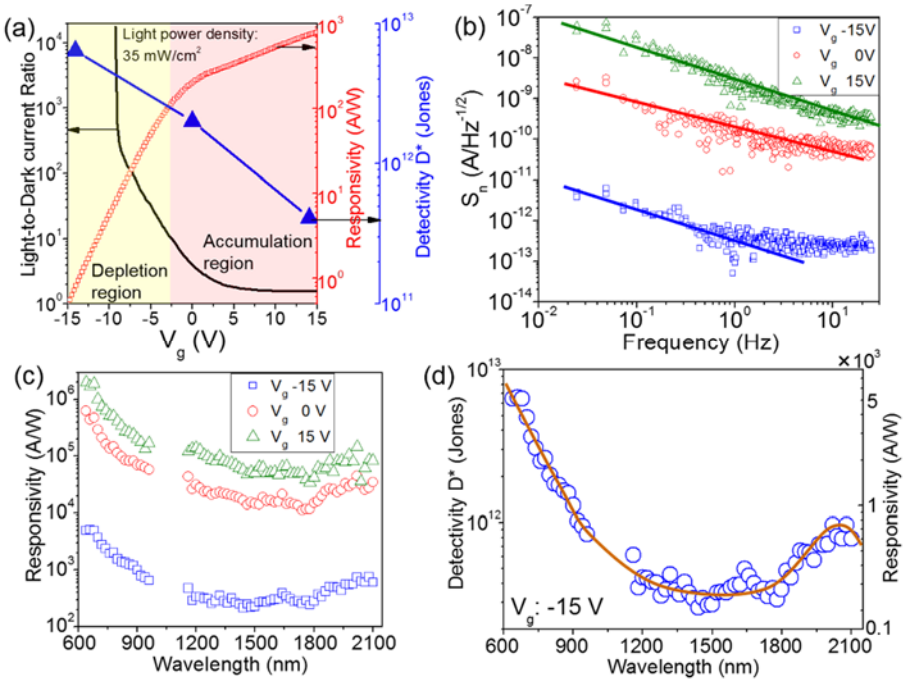

Figure 3. (a) Light-to-dark current ratio, Responsivity and measured D* as function of the backgate voltage with bias of 1 V and light illumination power density of 35 mW/cm^2 (corresponding to 7 nW light power on active area) with wavelength of 635 nm. (b) Noise spectral density (S_n) of the hybrid photodetectors under different backgate with V_{sd} of 1 V under ambient conditions at room temperature, the optimum noise spectral density is 3.5×10^{-13} A/$\sqrt{Hz}$ at 1 Hz under V_g of -15 V. The solid line is the 1/f fitting indicating dominated 1/f noise component in the detectors. The noise floor of the measuring unit is reached at V_g of -15 V and high frequency showing a flat spectral noise density line due to the lowest noise level measurable with our systems. (c) Spectral responsivities of the hybrid photodetectors at different backgate with bias of 1 V. (d) Wavelength dependence of the measured detectivity D* (at 1 Hz modulation frequency) and responsivity with measured bias and gate of 1 V and -15 V, respectively.